Optik - International Journal for Light and Electron Optics 181 (2019) 351–360

Contents lists available at ScienceDirect

Optik

journal homepage: www.elsevier.com/locate/ijleo

Original research article

Quality monitoring in wire-arc additive manufacturing based on cooperative awareness of spectrum and vision

Zhuang Zhao[a,1], Yiting Guo[a,1], Lianfa Bai[a], Kehong Wang[b], Jing Han[a,*]

[a] Jiangsu Key Laboratory of Spectral Imaging and Intelligent Sense, Nanjing University of Science and Technology, Nanjing 210094, China
[b] Department of Material Science and Engineering, Nanjing University of Science and Technology, Nanjing 210094, China

ARTICLE INFO

Keywords:
Quality monitoring
Cooperative awareness
Multi-source classification
Visual feature extraction
Spectral analysis

ABSTRACT

This paper presents a multi-source classification method based on cooperative awareness method of spectrum, vision and electrical parameter for the quality monitoring in wire-arc additive manufacturing. Triggered by the field programmable gate array (FPGA), the spectrum was collected in the peak current, and a weld pool image was captured in the base current. In this way, we acquired the multi-time information about both the spectrum with abundant information and the weld pool image with low interference within one welding current period, and achieved the cooperative awareness. We proposed a k-nearest neighbor (KNN) classification algorithm based on contour curve feature (CC-KNN) in vision and two classification methods -priori threshold and KNN based on locality preserving projection (LPP-KNN) -in spectral analysis. The combination of vision and spectrum can simultaneously monitor the unusual states of process parameters and quality defects. Our method is not limited to one welding process, and experimental results of three wire materials in cold metal transfer (CMT) welding have verified the superiority of our method on the number of monitoring objects, accuracy and stability.

1. Introduction

Addictive manufacturing (AM) is a developing technology which can reduce part cost and manufacture complex assemblies. The combination of an electric arc as heat source and wire as feedstock is referred to as Wire-arc additive manufacturing (WAAM) [1]. WAAM is one representative metal additive manufacturing technologies [2] in welding field. On-line quality monitoring of the weld pool has been a research topic in welding field as well as a main content of the intelligentized welding technology(IWT). In traditional manual quality monitoring, skilled welders rely on visual information and personal experience mainly to monitor the welding quality [3,4]. In order to simulate the welder's judgement of weld pool quality by observing the weld pool, many researchers have adopted the vision sensor to capture weld pool images [5]. These images contain abundant information and are closely related to the welding quality. Currently, the visual quality monitoring around the world is widely based on passive vision.

The passive vision sensing system of the weld pool, which does not need auxiliary light sources, uses the self-emitted radiation of the weld pool, the reflected light from the weld pool surface and the arc as the light sources. To capture clear images, this system uses the composite filter system with transmission wavelengths that have weak arc interference and strong weld pool self-emitted radiation. From, Wang et al. [6] found that the 1064 nm near-infrared bands are the best window to capture the weld pool image based on experimental results on four kinds of compound narrowband filters based on three kinds of mechanism. Yan et al. [7] further

* Corresponding author.
E-mail address: eohj@njust.edu.cn (J. Han).
[1] These authors contributed to the work equally and should be regarded as co-first authors.

https://doi.org/10.1016/j.ijleo.2018.12.071
Received 21 November 2018; Accepted 17 December 2018

pointed out that the 667 nm filter is a better choice since the 1064 nm filter is close to the longest monitoring wavelength of the CCD camera with weak sensitivity and poor imaging quality. Liang et al. [8] found that the 667 nm filter imaging method contains many external factors by analyzing imaging factors such as the weld pool, the arc radiation and the quantum efficiency of cameras.

As to the welding quality monitoring, weld pool images can be used to evaluate the weld pool's status, which is very intuitive in vision. However, due to the lack of comprehensive information, this method cannot solve problems related to the changes of material composition in welding process–the accurate shielding gas flow rate and the slag inclusion, for example. Thereby other measurement data is needed to used for this question. In welding, the shielding gas flow rate can influence fluidity of the weld pool and welding quality; besides, some precision machining, such as nuclear industry, has a strict requirement for the processing environment. So it is necessary to monitor the shielding gas flow rate and the interference of impurities. This paper used the arc spectrum to solve this problem. The arc spectrum, which includes abundant information about the weld pool characteristics, is from the excitation of the shielding gas ionizing, the welding wire gasification, etc. On-line spectral analysis system can simultaneously measure multi channels and multi components, with faster speed and higher accuracy. In arc additive manufacturing, because of the unaltered material components, each layer of the spectrum shows little difference.

In order to reduce the interference and meanwhile obtain abundant information, we used the field programmable gate array (FPGA) to trigger the CCD camera and the spectrometer. This method helps obtain multi-time information which contains a visual image captured in the base current and the spectral data collected in the peak current within one welding current period.

As mentioned above, we combined vision and spectrum by electrical parameter. In this way, we realized cooperative awareness of spectrum, vision and electrical parameter, solved problems related to the blind spots of monitoring, and maximized the categories of quality monitoring.

In terms of the processing of the weld pool images, most of weld pools' characteristics parameters in the quality monitoring are geometric parameters. Zhang et al. [9] proposed the polar coordinate model parameters such as length and two shape parameters, to determine the weld penetration. Chen et al. [10] used ten rear widths as shape parameters and used the maximum topside width, topside half-length and rear area as size parameters. Zhao et al. [11] proposed four parameters which are the length of the weld pool, the ratio of width of length, and shapes of the head and tail of the pool. Liu et al. [12] established that the model of the front side weld pool geometrical characteristic parameters is related to the welding current and speed. These parameters are weld pool length, width, convexity. Liu et al. [13] introduced the weld pool characteristic parameters about the weld pool width, the back of the weld pool length and the angle of the prop. To make full use of the quality information contained in the geometric shape of the weld pool, this paper proposed a contour curve (CC) feature.

As to arc spectral analysis, Shea et al. [14] monitored the intensity ratio of the hydrogen line in 656.28 nm and argon line in 696.54 nm to measure the 0.25% hydrogen in shielding gas. Mirapeix et al. [15] used a subpixel algorithm to calculate the plasma electronic temperature. This method can detect common defects in the welding seam caused by insufficient shielding gas flux or current fluctuations of the welding power source. Li et al. [16] detected some welding defects by using suitable spectral processing zones (250–300 nm, 750–830 nm, 776.6–777.6 nm, 867.5–868.5 nm, 900–1000 nm). García-Allende et al. [17] used sequential forward floating selection (SFFS) algorithm to realize spectral dimensionality reduction, and an artificial neutral network to carry out identification task. Zhang et al. [18] collected statistic characteristic parameters of certain spectrum bands of interest, adopted wavelet packet transform (WPT) to remove the pulse interference in the monitoring curves and used the signal-to-noise ratio (SNR) to monitor defects. In this paper, considering the quality monitoring contents and the spectral curve features, we adopted a method which combines the prior threshold with the k-nearest neighbor (KNN) based on locality preserving projection (LPP-KNN) method to process spectral data.

We used a multi-source classification method which combines the KNN classification algorithm based on CC feature (CC-KNN) with two spectral data processing methods, i.e. prior threshold-based method and LPP-KNN method. The multi-source classification based on the cooperative awareness of spectrum, vision, and electrical parameter is not limited to one welding process. In this paper, we used the cold metal transfer (CMT) welding process as an example, and verified the superiority of our method with the experimental results in the welding of stainless steel, high-strength steel and high-nitrogen steel.

2. Cooperative awareness

In this paper, we introduced a cooperative awareness method of spectrum, vision and electrical parameter. In this method, FPGA is used to achieve real-time acquisition of welding current parameters. Meanwhile, triggered by the FPGA, the spectral data was collected in the peak current, and the weld pool image was captured in the base current.

The schematic illustration and diagram of the cooperative awareness method is shown as Fig. 1. The system consists of three parts: FPGA device, data collecting device, and data storage and display device. FPGA device includes FPGA development board (ALINX XILINX spartan-6 XC6SLX9); the data collecting device includes: protective glass plate, 850 nm high pass filter, 10%neutral dimmer film, CCD camera (BASLER acA1920-155 um), spectrometer (ocean optics USB2000 +); and the data is stored and displayed on a computer.

During the process of capturing visual image, based on a lot of experiments, we find out that self-emitted radiation of weld pool and the reflected arc light of weld pool surface mainly gather around the near infrared band. Besides, there is only a small number of arc spectrum in the near infrared band. Thereby, we use 850 nm high pass filter to reduce the arc interference and increase the luminous flux of self-emitted radiation of weld pool. In addition, it can avoid the imaging quality degradation caused by low quantum efficiency of the camera. Thus, we can capture weld pool images with high quality.

During collecting spectrum, the working band of the spectrometer is 200–1100 nm, which suits the requirements of the quality

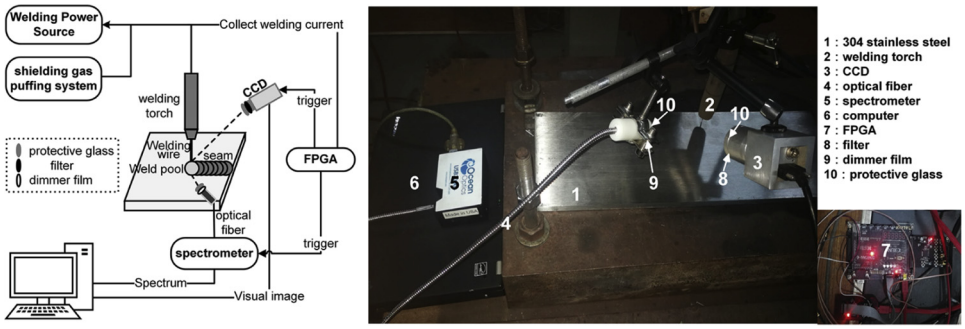

Fig. 1. Schematic illustration and diagram of the cooperative awareness method based on spectrum, vision and welding parameters.

monitoring.

This system is applicable to a variety of welding processes. In this paper, we used the CMT as an example, and the triggering time of the visual images and the spectrum is shown as Fig. 2:

High welding current results in strong arc interference. Thereby, the captured weld pool images are easily over exposed, while for certain wires (such as high-nitrogen steel), there is serious spatter. In order to avoid these problems, we captured the weld pool image in the base current.

As to the spectral data, there is no such problem related to the capturing of weld pool images. Since the arc spectrum is the radiation caused by the current excite the shielding gas and metal vapor, it is better to collect the spectrum in the peak current at which the arc is the strongest.

3. Quality monitoring based on vision

The stability monitoring of welding speed based on vision was performed when the welding current was obtained. For each kind of the welding currents, we arranged the corresponding classifier based on the welding currents acquired through the FPGA. This kind of quality monitoring is applicable to a wide range of welding wires. In this paper, we tested three welding wires, i.e. stainless steel, high-strength steel and high-nitrogen steel. The typical images of the three welding wires on 304 stainless steel base metal are shown as Fig. 3(a), (b), (c).

The welding speeds in the weld pool images are quite distinct from each other. Take the stainless steel wire at the fifth layer of the single-pass multi-layer welding and 25 L/min shielding gas flow rate as an example, the weld pool widths at different welding speeds are quite distinct from each other as shown in Fig. 4(a), (b), (c). As to the arc spectrum at different welding speeds, the component remains the same while only the intensity of the spectrum is changed. As shown in Fig. 4(d), although the relative intensities of Ar II (403.38 nm, 426.63 nm, 444.89 nm, 476.49 nm, 480.60 nm) and Ar I (518.77 nm, 696.54 nm, 706.72 nm, 737.21 nm, 750.39 nm, 763.51 nm, 772.37 nm, 810.36 nm) spectral lines are different, there is only minor difference of the relative intensities at the welding speed of 30 cm/min and 50 cm/min. Thereby the welding speed monitoring only dependent on vision.

3.1. Welding speed monitoring based on CC-KNN

CC-KNN algorithm extracts the curve features of the outer contour of the weld pool image and uses KNN [19], which is simple, reliable and highly stable [20], to classify the extracted features.

The welding speed monitoring consists of three parts: feature extraction, classification monitoring, and stability constraint.

To make full use of the difference of the contour of weld pool at different welding speeds, we used the contour curve of weld pool as the welding speed feature. The welding speed feature extraction includes: image enhancement, image segmentation, noise filter

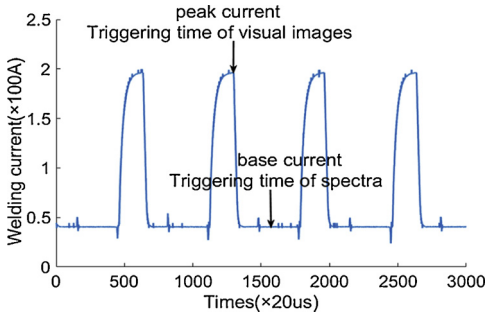

Fig. 2. Electrical signal diagram.

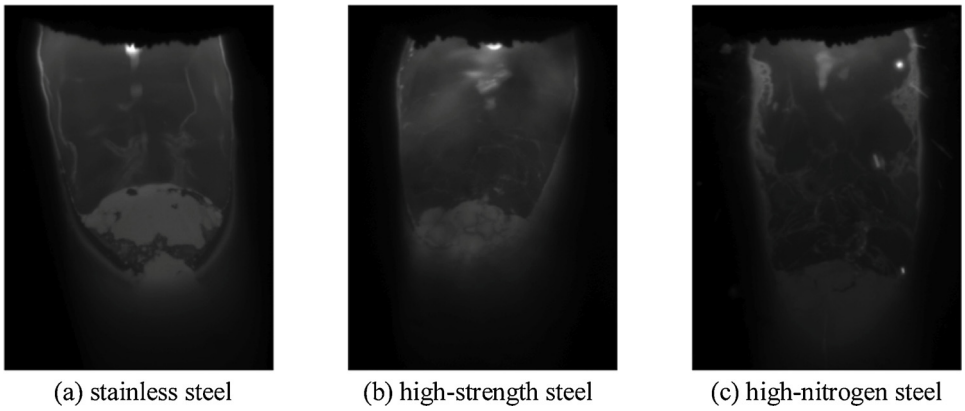

Fig. 3. weld pool image of different welding wires.

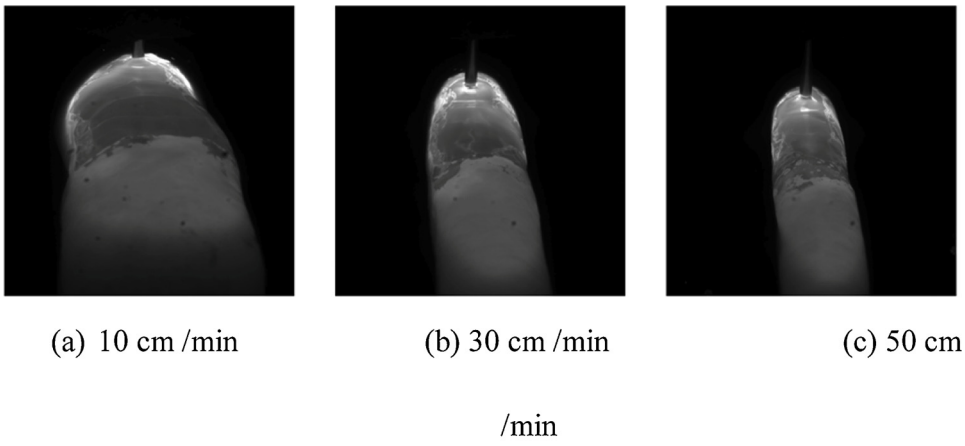

Fig. 4. Spectrum and weld pool images at different welding speeds.

and contour curve extraction.

In order to decrease the difficulty of image segmentation, we over exposed the weld pool when enhancing the weld pool image and transformed the product a of each gray value $\mathbf{g}_{oriange}(x, y)$ of the image and enhancement coefficient γ into each value $\mathbf{g}(x, y)$ of the enhanced image. The equation is:

$$a = \gamma \times \mathbf{g}_{oriange}(x, y)$$
$$\mathbf{g}(x, y) = \begin{cases} 255a \geq 255 \\ aa < 255 \end{cases} \quad (1)$$

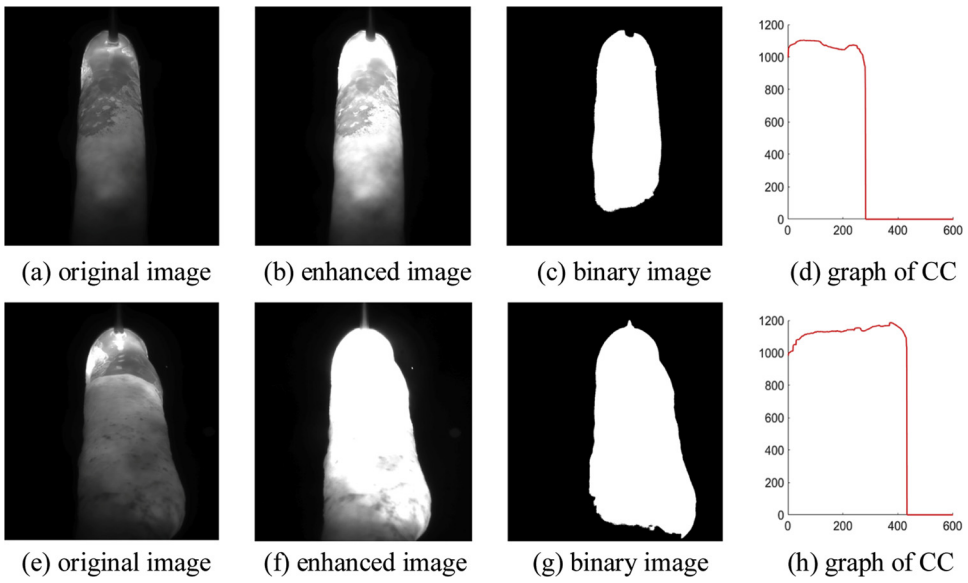

Fig. 5. Processing of weld pool images.

The Maximum Classes Square Error (OTSU) algorithm is used to perform image segmentation [21]. This algorithm is a highly efficient image binary algorithm whose selection criterion is based on the between-class variance of the maximum target and background.

The morphological noise filter uses the chain-coded method to measure the area of the connected regions. By keeping the largest region, i.e. the weld pool, the filter could effectively remove noises such as spatter.

CC contains the geometric information of the outer contour of the weld pool. Besides, CC also robustness to the identification error caused by visual angle changes. The equation is:

$$\begin{aligned} &\mathbf{m} = \arg\min \textstyle\sum_i \mathbf{I}_{i,j} > 0 \\ &\mathbf{n} = \arg\min \textstyle\sum_j \mathbf{I}_{i,j} > 0 \\ &\mathbf{O}_{i-m+1} = \arg\max \mathbf{I}_j = =1 \\ &\mathbf{V} = \mathbf{O} - \mathbf{n} \end{aligned} \tag{2}$$

where $\mathbf{V}$ is CC, $\mathbf{I}_{i,j}$ is the element of the row i and column j of the binary image after filtering, $\mathbf{m}$ ($\mathbf{n}$) is the smallest column index in which the sum of the column (row) vector elements of the binary image is larger than 0, and $\mathbf{O}_{i-m+1}$ is the largest row index in which the element of each column equals 1.

Take the stainless steel at the eighth layer of the single-pass multi-layer welding, 121 A welding current and 30 cm /min welding speed as an example, the curve diagram based on the image enhancement, binary image and the contour curve features is shown as Fig. 5. (a)–(d) are the original image, the enhanced image, the binary image, and the contour curve feature image at 25 L/min shielding gas flow rate. Fig. 5(e)–(h) are the same type of images of CC at 0 L/min shielding gas flow rate.

After the feature extraction of the contour of the weld pool, we used the KNN to realize the classification of welding speed.

Based on the continuous time series analysis of captured images of the same welding seam, we used the stability constraint to improve the stability and reliability of the classification results. According to stability constraint, the final recognition result of the image is decided by the majority voting of the recognition results of the images in the previous frames. We set the frame count to 3.

4. Quality monitoring based on spectrum

Take the stainless steel at the first layer of the single-pass multi-layer welding, 121 A welding current and 30 cm/min welding speed as an example, the discrimination of the weld pool images at 25 L/min and 5 L/min shielding gas flow rates is not obvious as shown in Fig. 6(a), (b); the discrimination of the weld pool images with or without rust and oil stain on the base metal at 25 L/min shielding gas flow rate is not obvious as shown in Fig. 6(c)–(f). The spectrum contains information about the material composition. Thereby the quality monitoring of shielding gas flow rate and residues on the base metal, such as oil stain and rust both, rely on spectral analysis.

We used two methods to analyze the spectral data:

1. As to the quality monitoring of spectrum that contains new material components, we analyzed the abnormal bands according to the atomic emission spectrum, selected specific bands and used threshold for the relative intensity of the spectrum or the ratio of the relative intensity to achieve quality monitoring;

2. As to the spectral curve, we first selected characteristic bands, then adopted the locality preserving projection (LPP) algorithm

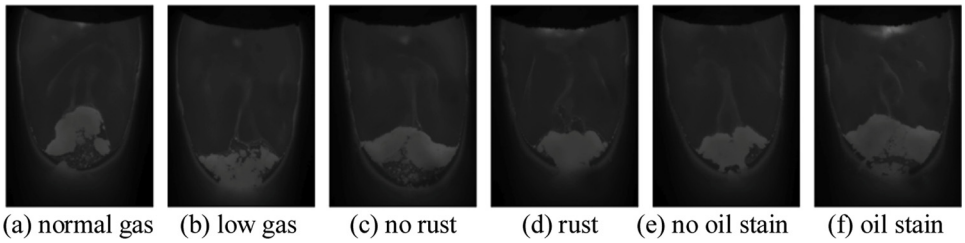

Fig. 6. Weld pool images with different defects.

[22] to further analyze the spectral information and used KNN to classify the final spectral features.

4.1. Quality monitoring of new material composition based on spectrum prior threshold

As to the quality monitoring of the spectrum that contains new material components such as base metal with or without rust and oil stain, we analyzed the specific spectral curve and then selected representative bands.

This quality monitoring can greatly reduce welding quality problems, such as poor weld formation, porous, rough surface, etc. These welding problems are caused by residual oil and rust due to improper cleaning and grinding during welding process. It is widely used in nuclear industry and ASME shipbuilding industry.

Iron oxide can form strong iron bands in 300–580 nm visible light [23]. We used the stainless steel at 25 L/min shielding gas flow rate, 30 cm/min welding speed and 121 A welding current as an example. The spectrum curve with or without rust is shown as Fig. 7(a). In the iron band, the relative intensity of spectrum with rust (Fe_2O_3) is higher than that without rust. Thereby, we applied a threshold for the average relative intensity of the normalized spectral data between 300–580 nm. If the average relative intensity is greater than the threshold for several times, it is concluded that rust exists.

The base metal with oil stain differs significantly from that without oil stain in the hydrogen spectrum. We used stainless steel at the first layer of the single-pass multi-layer welding, 25 L/min shielding gas flow rate, 30 cm/min welding speed and 121 A welding current as an example and the spectral curve is shown as Fig. 7 (b). The spectrum with oil stain displays obvious peaks in the hydrogen spectrum (656.28 nm). Besides, since the shielding gas contains oxygen, we concluded that the relative intensity of the oxygen spectrum (777.19 nm) remained the same. Thereby, we applied a threshold for the ratio of the relative intensity of the hydrogen spectrum and oxygen spectrum. If the average relative intensity is greater than the threshold for several times, it is concluded that oil stain exists.

4.2. Stability monitoring of shielding gas flow rate based on LPP-KNN

LPP-KNN classification, which is mainly used to monitor the shielding gas flow rate, uses the LPP dimensionality reduction to further analyze the characteristic bands and collect more spectral information, and then KNN is used to classify the final spectral features.

Take the stainless steel welding wire at the first layer of the single-pass multi-layer welding, 30 cm/min welding speed and 121 A welding current as an example, and the spectrum at different shielding gas flow rates is shown as Fig. 8. At different shielding gas flow rates, the material components remain unaltered. Thereby the first kind of spectrum processing method, which is used in the quality monitoring of new material components such as oil stain and rust, is not suitable for the shielding gas flow rate monitoring. If applied, the robustness will descend. When processing the spectrum, the LPP-KNN algorithm displays strengthened adaptability, increased stability in monitoring and stronger robustness while at the same time prevents the inaccurate classification caused by unsuitable threshold and current interference.

The LPP algorithm is based on the linear approximation of Laplacian Eigen maps [24]. The LPP algorithm, which is easy to use and fast in processing, can maintain the structure of local neighborhood of the samples in space when performing data dimensionality reduction.

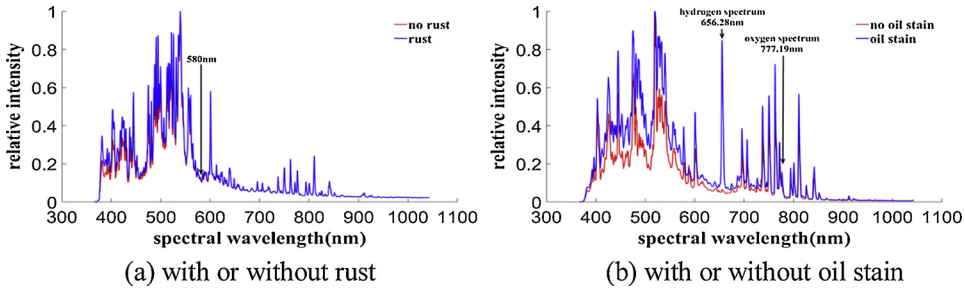

Fig. 7. Spectrum with different defects.

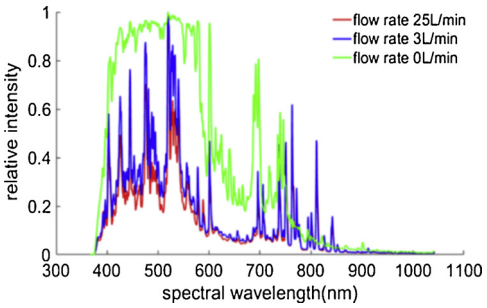

Fig. 8. Spectrum at different shielding gas flow rates.

Suppose the number of n dimension sample sets $\mathbf{X} = \{x_1, x_2, \cdots, x_m\}$, where $x_i \in \mathbf{R}^n (i = 1, \cdots, m)$, is m, and the goal of the LPP algorithm is to use the projection matrix $\mathbf{W} = \{w_1, w_2, \cdots, w_l\}$, l<n to project the data sets $\mathbf{X}$ onto a low-dimensional feature space $\mathbf{Y} = \{y_1, y_2, \cdots, y_m\}$, where $y_i \in R^l (i = 1, \cdots, m)$, i.e. $y_i = \mathbf{W}^T x_i$. LPP algorithm identifies the optimal projection direction by minimizing the objective function.

$$\min \sum_{i,j} || y_i - y_j ||^2 \mathbf{S}_{ij} \tag{3}$$

We used the Kernel-weighted method to obtain the weight matrix $\mathbf{S}$, and the equation is:

$$\mathbf{S}_{i,j} = \begin{cases} \exp(-|| x_i - x_j ||^2 / t) x_i and x_j are neighbors \\ 0 otherwise \end{cases} \tag{4}$$

The function can be simplified into generalized eigenvalue problem as:

$$X\mathbf{L}\mathbf{X}^T w = \lambda X \mathbf{D}\mathbf{X}^T w \tag{5}$$

where $\mathbf{D}$ is the diagonal matrix, and the elements on the diagonal line is the sum of the rows (or the columns) of the weight matrix, i.e. $\mathbf{D}_{ii} = \sum_{j=1}^{n} \mathbf{S}_{ij}$. $\mathbf{L}$ is the Laplacian symmetric semidefinite matrix, $\mathbf{L} = \mathbf{D} - \mathbf{S}$. w is the eigenvector, λ is the eigenvalue.

After LPP dimensionality reduction, we used KNN classifier to perform shielding gas flow rate monitoring.

5. Experiments and results

5.1. Experimental setup

Experimental devices include: an intelligent welding robot; FRONIUS CMT Advanced 4000Rnc welding power source; shielding gas puffing system; welding bench; stainless steel, high-strength steel, and high-nitrogen steel welding wires; 304 stainless steel base metal; cooperative awareness of spectrum, vision and electrical parameter.

Experimental conditions of quality monitoring are shown as Table1:

For the stainless steel welding wire, the normal welding current is 121 A; for the high-strength steel and the high-nitrogen steel, the normal welding current is 130 A. The shielding gas consists of 98.5% argon and 1.5% oxygen. The total sample sizes in stainless steel, high-strength steel and high-nitrogen steel welding wires experiments are 9800, 13,300 and 12200, respectively. 30% of these total samples are randomly sampled as train samples. These samples were collected at different times, which thereby are representative and can verify the stability of our method.

Flowchart of the quality monitoring is shown as Fig. 9:

5.2. Experimental results of welding speed

As to the sample collection of welding speed data sets based on visual images, the experimental conditions are shown as Table 2:

Fig. 10 is the result of the welding speed monitoring of three different welding wires in which we analyzed 7 features, i.e. the Local Binary Patter (LBP) [25], the Histogram of Oriented Gradient (HOG) [26], the weld pool width, the weld pool length, the weld pool area, fusion feature of length, width and area(FF-LWA), and contour curve(CC). Four classifiers are employed here, i.e. KNN, Naive Bayes(NB) [27], Adaptive Boosting based on decision Tree (AdaboostM2-DT) [28], and the combination approach of Error-Correcting Output Codes and Supported Vector Machine (ECOC-SVM) [29]. As shown in Fig. 10, compared with other methods, the

Table 1
Experimental condition of quality monitoring.

Welding method	Welding process	Camera exposure	Welding current
single-pass multi-layer welding	CMT	600 us	Normal

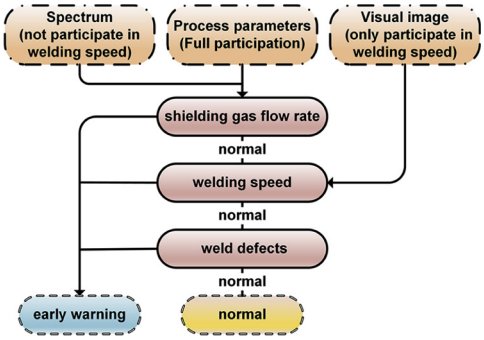

Fig. 9. Flowchart of quality monitoring.

Table 2
Experimental conditions of welding speed data sets.

Welding wire	Welding current (A)	Welding speed (cm/min)	Shielding gas (L/min)
Stainless steel	121	10/30/50	25
High-strength steel	130	15/30/45	25
High-nitrogen steel	130	15/30/45	25

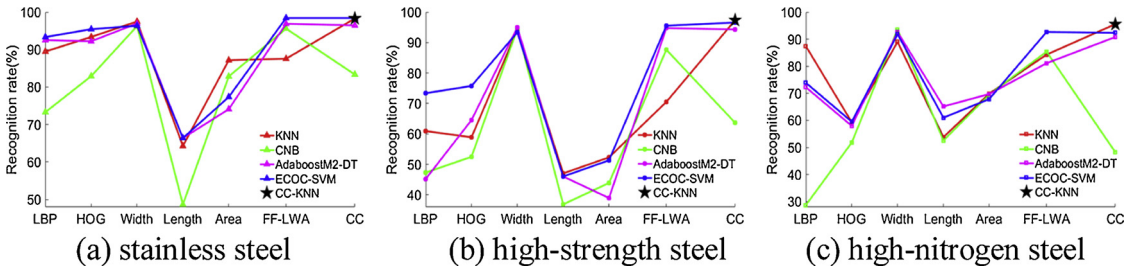

Fig. 10. Experimental results of different welding speeds.

CC-KNN we proposed in general yields best performance.

5.3. Experimental results of shielding gas flow rate

Table 3 is the experimental results of three welding wires at different shielding gas flow rates and under different data dimensionality reduction methods. The shielding gas flow rates are 0 L/min, 3 L/min, 25 L/min. The three data dimensionality reduction methods are: Linear Discriminant Analysis (LDA) [30], LPP and Multi-Manifold Discriminant Analysis (MMDA) [31]. As shown in Table 3, LPP-KNN achieve best performance.

5.4. Experimental results of new material composition

As to the normalized spectral data, we applied a threshold for the average relative intensity in strong iron bands (300–580 nm) of visible light, and then detected the rust on the base metal. Fig. 11(a) is the analysis result of stainless steel base metal in single-pass multi-layer welding in which the middle part is spread with pure rust powder and the appearance of weld bead with rust defect. After several experiments, we set the threshold to 0.32. When the ratio is larger than 0.32 for three times, it is concluded that rust exists in the base metal.

We applied a threshold for the ratio of the relative intensity of hydrogen (656.28 nm) characteristic spectrum and oxygen

Table 3
Experimental results at different shielding gas flow rates.

Welding wire	stainless steel(%)	high-strength steel (%)	high-nitrogen steel(%)
LDA-KNN	81.81	92.24	88.95
LPP-KNN	**98.90**	**96.85**	**99.95**
MMDA-KNN	81.83	32.68	81.59

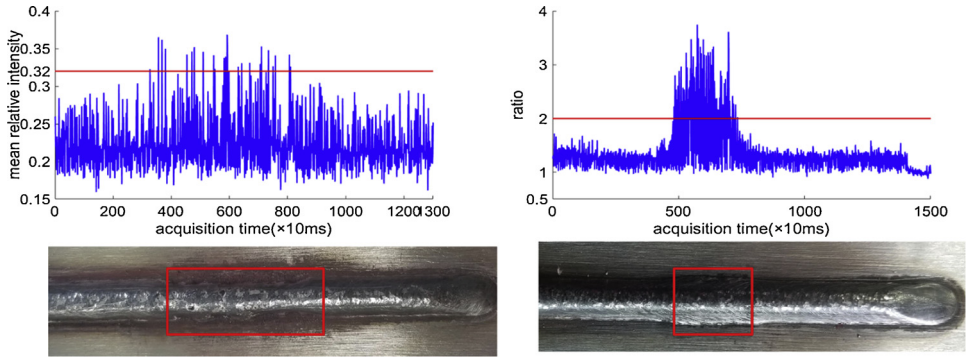

Fig. 11. Experimental results of different defects and welding appearance.

(777.19 nm) characteristic spectrum and then detected the oil stain on the base metal. Fig. 11(b) is the analysis result of the spectral data of base metal in single-pass multi-layer welding with oil stain in the middle part and the appearance of weld bead with oil stain defect. After several experiments, we set the threshold to 2. If the ratio is larger than 2 for five consecutive times, it is concluded that oil stain exists in the base metal.

6. Conclusion

In this paper, we proposed a cooperative awareness method of spectrum, vision and electrical parameter. Triggered by the FPGA, the spectrum was collected in the peak current, and the weld pool image was captured in the base current within one welding current period. In this way, we obtained the multi-time information which outperforms the single spectrum or vision with abundant information. CC was proposed in this paper, which contains more information about the welding speed. Compared with geometric features such as weld pool width, length, area and texture features such as LBP and HOG, CC achieve better performance when used to monitor the welding speed. The visual classification algorithm CC-KNN and spectral analysis of two classification methods, including priori threshold and LPP-KNN, can effectively perform quality monitoring of the weld pool. The combination of vision and spectrum can make full use of the multi-source information. In this way, it not only makes up for the weaknesses of spectral analysis on welding speed but also solves the short board of the monitoring at low shielding gas flow rate and the detection of new material composition in vision. The experimental results of stainless steel, high-strength steel, and high-nitrogen steel based on CMT welding process have verified that multi-source online quality monitoring of the weld pool can detect more quality problems and has higher recognition rate than single-source monitoring.

Limited by the actual band range and the sensitivity of the spectrometer, further research on the quality monitoring of spectrum with a small amount of doping is needed to improve the recognition rate. Besides, since in this paper the welding method is limited to the surfacing welding, other welding methods such as fillet welding need to be further researched.

Acknowledgements

This work was supported by the National Natural Science Foundation of China (no. 61727802 and 61501235).

References

[1] S.W. Williams, F. Martina, A.C. Addison, J. Ding, G. Pardal, P. Colegrove, Wire + arc additive manufacturing, Mater. Sci. Technol. 7 (2015) 641–647.
[2] X. Shi, S. Ma, C. Liu, Q. Wu, J. Lu, Y. Liu, et al., Selective laser melting-wire arc additive manufacturing hybrid fabrication of ti-6al-4v alloy: microstructure and mechanical properties, Mater. Sci. Eng. A 684 (2017) 196–204.
[3] Y.K. Liu, Y.M. Zhang, L. Kvidahl, Skilled human welder intelligence modeling and control: part 1 – modeling, Weld. J. 93 (5) (2014).
[4] R. Kovacevic, Y.M. Zhang, Machine vision recognition of weld pool in gas tungsten arc welding, *Proceedings of the Institution of Mechanical Engineers Part B Journal of Engineering Manufacture* 209 (22) (1995) 141–152.
[5] B. Guo, Y. Shi, G. Yu, B. Liang, K. Wang, Weld deviation detection based on wide dynamic range vision sensor in mag welding process, Int. J. Adv. Manuf. Technol. 87 (9-12) (2016) 3397–3410.
[6] K. Wang, X. Tang, Y. Liu, Y. Xu, J. Yu, Experimental research on the method of vision detecting mag welding pool information, Chin. J. Mech. Eng. 40 (6) (2004) 161–164.
[7] Z.H. Yan, G.J. Zhang, M.Z. Qiu, H.M. Gao, L. Wu, Monitoring and processing of weld pool images in pulsed gas metal arc welding, Trans. China Weld. Instit. 26 (2) (2005) 37–40.
[8] Z. Liang, S. Zhao, M. Zhang, H. Gao, Vision sensing of weld pool for p-gmaw by an infrared transmitting filter, Trans. China Weld. Inst. 35 (2) (2014) 33-36 + 41.
[9] Y.M. Zhang, R. Kovacevic, L. Li, Characterization and real-time measurement of geometrical appearance of the weld pool, Int. J. Mach. Tools Manuf. 36 (7) (1996) 799–816.
[10] S.B. Chen, D.B. Zhao, L. Wu, L.J. Lou, Intelligent methodology for sensing, modeling and control of pulsed gtaw: part 2 - butt joint welding, Weld. J. 79 (6) (2000) 164-s.
[11] D.B. Zhao, S.B. Chen, L. Wu, Q. Chen, Shape parameter definition and image processing of the weld pool during pulsed gtaw with wire filler, Trans. China Weld. Instit. 22 (2) (2001) 5–8.
[12] Y.K. Liu, Y.M. Zhang, Adaptive modeling of the weld pool geometry in gas tungsten arc welding, IEEE International Conference on Networking, Sensing and Control (2013) pp.550-555.

[13] X. Liu, X. Ji, Weld Pool image processing and feature extraction based on the vision of the CO2 welding, *Proceedings of the 4th International Conference on Computer Engineering and Networks*, Springer International Publishing, 2015.
[14] J.E. Shea, C.S. Gardner, Spectroscopic measurement of hydrogen contamination in weld arc plasmas, J. Appl. Phys. 54 (9) (1983) 4928–4938.
[15] J. Mirapeix, A. Cobo, O.M. Conde, Real-time arc welding defect detection technique by means of plasma spectrum optical analysis, Ndt E Int. 39 (5) (2006) 356–360.
[16] Z. Li, B. Wang, J. Ding, Detection of gta welding quality and disturbance factors with spectral signal of arc light, J. Mater. Process. Technol. 209 (10) (2009) 4867–4873.
[17] P.B. García-Allende, J. Mirapeix, O.M. Conde, A. Cobo, J.M. López-Higuera, Spectral processing technique based on feature selection and artificial neural networks for arc-welding quality monitoring, Ndt E Int. 42 (1) (2009) 56–63.
[18] Z. Zhang, H. Yu, N. Lv, S. Chen, Real-time defect detection in pulsed gtaw of al alloys through on-line spectroscopy, J. Mater. Process. Technol. 213 (7) (2013) 1146–1156.
[19] T. Cover, Nearest neighbour pattern classification, IEEE Trans. Inf. Theory 13 (1967).
[20] M. Mejdoub, C.B. Amar, Classification improvement of local feature vectors over the knn algorithm, Multimed. Tools Appl. 64 (1) (2013) 197–218.
[21] N. Otsu, A threshold selection method from gray-level histograms, IEEE Trans. Syst. Man Cybern. 9 (1) (2007) 62–66.
[22] X. He, Locality preserving projections, Adv. Neural Inf. Process. Syst. 16 (1) (2003) 186–197.
[23] T. He, J. Wang, Y. Chen, Z.J. Lin, Study on spectral features of soil fe_2o_3, Geogr. Geo-Inf. Science 22 (2) (2006) 30–34.
[24] X. He, S. Yan, Y. Hu, P. Niyogi, H.J. Zhang, Face recognition using laplacianfaces, IEEE Trans. Pattern Anal. Mach. Intell. 27 (2005) pp.328–340.
[25] T. Ahonen, A. Hadid, M. Pietikäinen, Face recognition with local binary patterns, European conference on computer vision, 2004, ECCV 2004, Lecture Notes in Computer Science 3021 Spring, 2004, pp. 469–481.
[26] N. Dalal, B. Triggs, Histograms of oriented gradients for human detection. Computer vision and pattern recognition, 2005. CVPR 2005, IEEE Computer Society Conference on (1, Pp.886-893). IEEE, (2005).
[27] Q. Wang, G.M. Garrity, J.M. Tiedje, J.R. Cole, Naïve bayesian classifier for rapid assignment of rrna sequences into the new bacterial taxonomy, Appl. Environ. Microbiol. 73 (16) (2007) 5261.
[28] T.G. Dietterich, An experimental comparison of three methods for constructing ensembles of decision trees: bagging, boosting, and randomization, Mach. Learn. 40 (2) (2000) 139–157.
[29] G. Zheng, Z. Qian, Q. Yang, C. Wei, X. Lu, Y. Zhu, et al., The combination approach of svm and ecoc for powerful identification and classification of transcription factor, BMC Bioinformatics 9 (1) (2008) 1–8.
[30] W.S. Zheng, J.H. Lai, S.Z. Li, 1d-lda vs. 2d-lda: when is vector-based linear discriminant analysis better than matrix-based? Pattern Recognit. 41 (7) (2008) 2156–2172.
[31] W. Yang, C. Sun, L. Zhang, A multi-manifold discriminant analysis method for image feature extraction, Pattern Recognit. 44 (8) (2011) 1649–1657.